

Deep learning improved by biological activation functions

G.S. Bhumra*

***Address:** Department of Neuroscience, Physiology and Pharmacology, UCL, Gower Street London WC1E 6BT, UK

Corresponding author: G.S. Bhumra (g.bhumra@ucl.ac.uk)

Abstract

'Biologically inspired' activation functions, such as the logistic sigmoid, have been instrumental in the historical development of machine learning techniques. However in the field of deep learning, they have been largely displaced by rectified (ReLU) or exponential (ELU) linear units to mitigate the effects of vanishing gradients associated with error back-propagation. The logistic sigmoid however does not represent the true input-output relation under physiological conditions. Here, radical root unit (RRU) activation functions are introduced, exhibiting input-output non-linearities that are substantially more biologically plausible since their functional form is based on known current-frequency relationships.

In order to evaluate whether RRU activations improve deep learning performance, networks are constructed with identical architectures except differing in their transfer functions (ReLU, ELU, and RRUs). Multilayer perceptrons, stacked auto-encoders, and convolutional networks are used to test supervised and unsupervised learning based on the MNIST dataset. Results of learning performance, quantified using loss and error measurements, demonstrate that the RRU networks not only train faster than their ReLU and ELU counterparts, but also lead to improved generalised models in the absence of formal regularisation. These results therefore confirm that revisiting the properties of biological neurones and their circuitry might prove invaluable in the field of deep learning.

1 Introduction

Neurobiology has inspired the design of computational networks ever since they were first conceived (Hassabis et al., 2017). When the ‘perceptron’ classifier was introduced (Rosenblatt, 1958), the non-linearity that described the input-output relationship was based on a critical input boundary above which outputs were fully activated resembling the ‘threshold’ and ‘all-or-none’ properties of neurones (Hodgkin and Huxley, 1952). Continuous ‘activation’ or ‘transfer’ functions, such as the sigmoid non-linearity (Figure 1), were subsequently adopted to represent the output of units as analogous to neuronal firing rates (Dayan and Abbott, 2001). With the advance of deep learning however ‘biologically-inspired’ activation functions have been largely supplanted by non-linearities that possess a linear component in the positive polarity (Nair and Hinton, 2010, Glorot et al., 2011). An advantage of these more recent transfer functions, notably the rectified linear unit (ReLU, Figure 1), is that their non-contractive positive activations mitigate the effects of vanishing gradients associated with error back-propagation. Since the deep learning performance of ReLU activation function and its variants usually exceed that of their sigmoid predecessors that confer no such advantage, the utility of ‘biological insights’ into input-output relationships might be called into question.

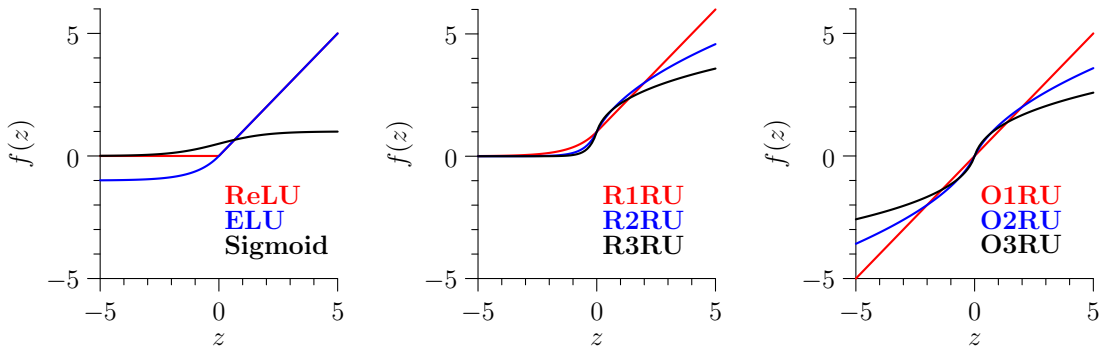


Figure 1: Graphs of activation functions. The left overlays the standard logistic sigmoid function, rectified linear unit (ReLU), and exponential linear unit (ELU). Middle and right plots overlays the RRRU and ORRU activations functions for $r = \{1, 2, 3\}$.

Electrophysiological recordings (Binder et al., 2011) and biophysical simulations (Fourcaud-Trocmé et al., 2003, Bhumbra et al., 2014) of neurones however show that their input-output relationships are not sigmoid. At rheobase, which defines the minimum input current required to evoke a single output discharge, only modest increments in depolarising inputs are required to accelerate firing in many neuronal types. This acceleration results from active conductances, mediated by voltage-sensitive ion channels, that overcome passive leak conductances and drive neuronal firing. However, after an initial linear slope in the input-output relation, the response curve only partially saturates as the voltage-sensitive channels become increasingly inactivated. While experimentally induced depolarisation can inactivate these channels completely, consistent with the theoretical concept of a maximum output discharge rate, this depolarisation is well beyond the physiological range. To suggest therefore this biological input-output relationship must therefore constitute a fully saturating activation function represents as little useful scientific insight as the suggestion that the ReLU activation must saturate in practice due to the finite numeric range of computer floating point units.

Here, a family of transfer functions termed radical root units (RRU), are introduced which are substantially more biologically plausible than sigmoid activations. The RRU comprises two subfamilies, namely the rectified radical roots units (RRRU) and odd radical root units (ORRU) which can be combined for different layers within a deep network. The performance of RRU networks is compared to that of identical networks that differ only in their activation using either the ReLU transfer function or one of its variants (Clevert et al., 2015) called the ‘exponential linear unit’ (ELU, Figure 1).

2 Methods

2.1 Radical root units

The rectified radical root unit (RRRU) is:

$$f(z) = \begin{cases} (r^2z + 1)^{\frac{1}{r}} - 1, & \text{if } z \geq 0 \\ e^{rz}, & \text{if } z < 0 \end{cases}, \quad \frac{df(z)}{dz} = \begin{cases} r(r^2z + 1)^{\frac{1-r}{r}}, & \text{if } z \geq 0 \\ re^{rz}, & \text{if } z < 0 \end{cases} \quad (1)$$

where the radix r is a positive shape parameter that defines the choice of non-linearity. The RRRU is monotonic and its derivative is continuous everywhere including at $z = 0$, where the derivative is at its maximum r . A radical function was chosen on the basis of the successful use of square root functions to fit current-frequency relationships observed in current-clamp recordings from neurones (Ermentrout, 1998) and those obtained from biophysical models (Fourcaud-Trocmé et al., 2003). This is analogous to an RRRU with a radix r of 2, which is termed the rectified 2nd root unit (R2RU, Figure 1). The first root (R1RU, Figure 1) is identical to the ELU transfer function incremented by one. For higher root units, the derivative is decreasing in the positive polarity but does not asymptote to zero, unlike in the negative polarity. At the limit where $r \rightarrow \infty$, the RRRU tends towards a Heaviside step function.

Whereas RRRU activations are only positive, the related odd radical root unit (ORRU) also produces negative values:

$$f(z) = \text{sgn}(z)((r^2|z| + 1)^{\frac{1}{r}} - 1), \quad \frac{df(z)}{dz} = r(r^2|z| + 1)^{\frac{1-r}{r}} \quad (2)$$

where once again the radix r is a positive shape parameter that defines the choice of non-linearity. Like the RRRU, the ORRU is monotonic and its derivative is continuous everywhere including at $z = 0$, where the derivative is at its maximum r . However unlike the RRRU, the symmetrical functional form of the ORRU makes the activation function odd. The first root (O1RU, Figure 1) corresponds to the identity function. For higher root units, the magnitude of the derivative decreases in both polarities but does not asymptote to zero. Therefore while the profile of ORRU functions may resemble the hyperbolic tangent, their activations are not asymptotically bounded.

2.2 Weight coefficient initialisation

Methods of initialising weight coefficients based on scaling second moments (Glorot and Bengio, 2010) aim to regulate variances of activations propagated throughout hidden layers. Recent optimisation of this technique for ReLU networks (He et al., 2015) adopts a Gaussian initialisation with variances scaled by $2/n_i$, where n_i is the number of inputs. For RRU networks, a single variance scaling initialisation cannot apply while preserving the freedom of adopting a range of RRU non-linearities throughout different layers. For this reason an empirical approach, consistent with synaptic neurophysiology, is adopted in assigning weights with the aim of distributing inner products to strategic domains within the derivative of the corresponding activation function to optimise back-propagation of gradients.

ReLU activations are bimodal with a first mode at $z = 0$ and a second skewed mode. Since similar skews are inevitable for RRRU activations and their derivatives are highly asymmetric, a skewed distribution is selected for assigning weights. By analogy, the distribution of biological post-synaptic responses to a single synaptic vesicle exhibits a characteristic skewed unimodal distribution (MacLachlan, 1975). Since these distributions are well described using a gamma probability density

function (Robinson, 1976, Bhumbra and Beato, 2013), RRRU weight initialisation is assigned using a gamma distribution.

$$\mathcal{G}(v|\gamma, \lambda) = \frac{1}{\lambda^\gamma \Gamma(\gamma)} v^{\gamma-1} e^{-v/\lambda}, \quad \Gamma(\gamma) = \int_0^\infty g^{\gamma-1} e^{-g} dg \quad (3)$$

where γ and λ are the shape and scale parameters respectively. The shaping parameter γ is set according to the non-linearity radix r by mapping a measure of skewness based on the quotient of the mean over the mode for v , to quantify the asymmetry in the activation derivative for z given in Equation 1. This asymmetry is expressed with respect to the relative positions of z for the two polarities where the derivative on the positive side coincides with the derivative at a fixed negative value for z . Setting this fixed value to $z = -1/e$ (details in the Appendix), the resulting inter-relation between γ and r is:

$$\gamma = 1 + \frac{r^2}{e \left(\exp \left(\frac{r^2}{e(r-1)} \right) - 1 \right)} \quad (4)$$

When r is one, the fraction term equates the zero and therefore results in a γ of one corresponding to an exponential probability density function. The remaining parameter λ determines the variance in the form $\sigma^2 = \gamma\lambda^2$. As r increases, the high magnitude RRRU derivatives are distributed either side of $z = 0$ over decreasing regions in z . Therefore rather than attempting to adopt a single standardisation for variance scaling coefficients, they are assigned according a reciprocal relation with the radix: $\sigma^2 = 3/(r+1/2)$. For R1RU initialisations ($r = 1$), this results in an identical variance scaling as suggested by He et al. (2015). The scaling parameter λ can be expressed with respect to γ and r .

$$\lambda = \sqrt{\frac{3}{\gamma(r + 1/2)}} \quad (5)$$

The values for v are recentered to a mean of zero by the first moment ($\gamma\lambda$) before implementing the ‘fan-in’ convention of scaling to the number of inputs n_i :

$$w = \frac{v - \gamma\lambda}{\sqrt{n_i}} - \frac{1}{n_i} \quad (6)$$

where the final subtraction, by $1/n_i$, offsets the weight coefficients by a small degree resulting in rectified activations closer to zero. This alleviates undesirable bias shift effects, particularly for the first hidden layer or other RRRU layers receiving inputs that are only or mostly positive, on gradient propagation that would impede learning (Clevert et al., 2015).

Initialisation for ORRU layers requires no skewed distribution due to the odd functional form resulting in activations with two modes either side of $z = 0$. While weights can be assigned according to a Gaussian distribution, platykurtic distributions, such as truncated Gaussians, are often used in practice to bound values and avoid extreme outliers. By analogy, at biological pre-synaptic terminals the probabilities of vesicular release are typically heterogenous, bounded within the range $[0, 1]$, and with a distribution that is usually platykurtic (Murthy et al., 1997). Since these distributions are well described using a beta probability density function (Silver, 2003, Bhumbra and Beato, 2013), which is closely related to the gamma distribution, ORRU weight initialisation is assigned using a beta distribution.

$$B(v|\alpha, \beta) = \frac{v^{\alpha-1}(1-p)^{\beta-1}}{B(\alpha, \beta)}, \quad B(\alpha, \beta) = \frac{\Gamma(\alpha)\Gamma(\beta)}{\Gamma(\alpha + \beta)} \quad (7)$$

In the case of a symmetrical distribution the two parameters equate ($\alpha = \beta$), and its profile becomes more Gaussian as α and β increase in value. For simplicity, a symmetrical beta distribution is assigned for ORRU weight initialisation according to Equation 4 where $\alpha = \beta = \gamma$. When r is one, the fraction term again equates to zero and therefore results in a beta distribution of $\alpha = \beta = 1$ corresponding to an uniform probability density function.

Since the ORRU derivative is symmetrically distributed about $z = 0$ over a domain in z that differs to that for the equivalent RRRU derivative, the variance scaling is different and given by the simpler relation: $\sigma^2 = 2/r$. For O1RU initialisations ($r = 1$), this again results in an identical variance scaling as suggested by He et al. (2015). Since the second moment of the beta distribution is already determined by α and β , the rescaling is performed as part of the $w = f(u)$ transformation by first subtracting u by the first moment of a symmetric beta distribution (0.5) then pre-scaling by its known corresponding standard deviation: $(8\alpha + 4)^{-1/2}$.

$$w = \frac{(v - 0.5)\sqrt{16\alpha + 8}}{\sqrt{rn_i}} \quad (8)$$

For RRU networks, output layers employing softmax or sigmoid functions are initialised in the same way as for O1RU activations, which corresponds to a uniform distribution. For the experiments described in the present study, ReLU and ELU network weight coefficients were initialised using fan-in variance scaling (He et al., 2015). In all layers with weight coefficients, bias offset parameters were trainable and initialised to $\mathbf{b} = 0$. All experiments were conducted using the TensorFlow machine learning framework (Abadi et al., 2015).

3 Results

3.1 Multilayer perception supervised learning

Since two subfamilies of activations functions as well as the corresponding weight initialisation regimens presented in this study are entirely novel, simple experiments were first conducted to confirm that RRU non-linearities facilitate deep learning. Fully connected multilayer perceptron networks of varying depth, from 4 to 8 hidden layers, were trained on the MNIST data set (55000 training and 10000 test data). In order to allow comparisons with previous work (Clevert et al., 2015), the architectures and training parameters were matched with 128 units in each hidden layer, a learning rate of 0.01, a batch size of 64, a softmax output activation, a cross entropy loss function, and a stochastic gradient descent learning update. In correspondence with the MNIST dataset dimensionality, the input data dimension was 784, and the number of output units was 10.

Transfer functions for hidden layers were either ReLU, ELU, or RRU functions. The subtypes of RRU were assigned according to the following scheme: R3RU for the first hidden layer, R1RU for the last hidden layer, and O2RU for intervening hidden layers. This order was chosen to minimise diminishing gradients during back-propagation and to center activations in the middle hidden layers around zero. Training and test loss values are plotted for each the three types of networks in Figure 2.

Training cross entropy losses plotted in the top row of Figure 2 show that with 4 hidden layers, the ELU network is the slowest in training. The ReLU network is somewhat faster whereas by a substantial

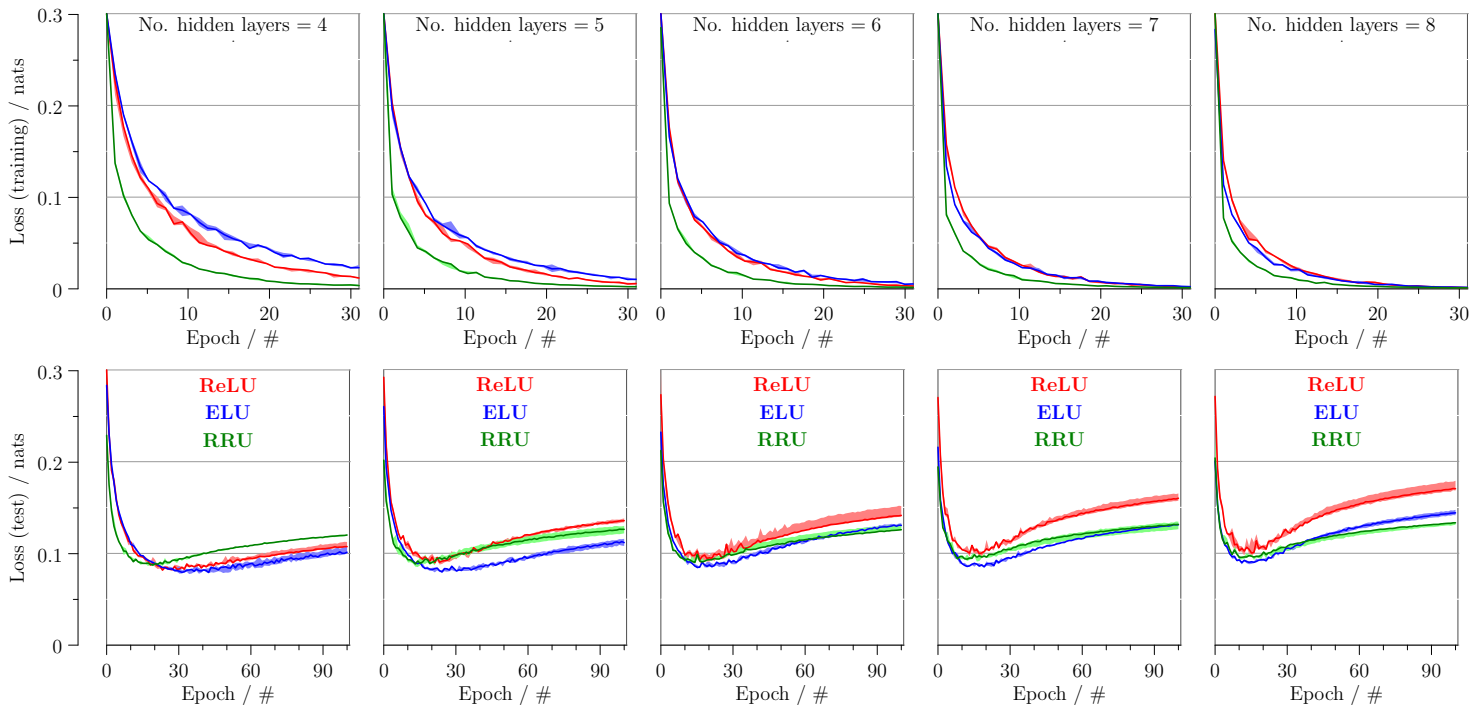


Figure 2: Multilayer perceptron training on the MNIST data set with 4 to 8 hidden layers. Networks employing ReLU, ELU, and RRU activation functions were trained, and the loss for training and test sets from several runs are plotted as lines for the medians and bands for the inter-quartile ranges.

margin the RRU network is the fastest. With 6 hidden layers, the training performance of the ReLU and ELU networks have both improved with comparable training loss profiles but the RRU network remains considerably faster. For the 8 hidden layer network, which repeats precisely the experiment of Clevert et al. (2015), the ELU network outperforms the ReLU network, confirming the findings of the previous study; the RRU network however still maintains its notable lead as the fastest learning network of the three.

Test cross entropy losses plotted in the bottom row of Figure 2 show that with 4 hidden layers, in the initial stages of learning ReLU and ELU networks are comparable in generalisation during learning. While the RRU network shows the fastest reduction in test loss, it is also the first to exhibit subsequent increases in test loss indicative of overfitting. As the number of hidden layers increase, the ReLU and ELU networks increasingly overfit with the ReLU networks being the most sensitive. By contrast, overfitting from the RRU networks is minimally affected by changes in the number of hidden layers. This suggests that the intrinsic capability of RRU networks to learn generalised models is resistant to the adverse effects of overfitting resulting from increases in depth within the network even in the absence of explicit regularisation.

3.2 Stacked auto-encoder unsupervised learning

Following the superior performance of RRU multilayer perceptron networks in supervised learning, a similar experiment was performed to assess unsupervised learning using a stacked auto-encoder network. A standard auto-encoder network design (Hinton and Salakhutdinov, 2006, Desjardins et al., 2015, Clevert et al., 2015) was implemented using a symmetrical architecture with [1000, 500, 250, 30, 250, 500, 1000] units that include both encoder and decoder components with 784 inputs and 784 output units for the MNIST image data. Training parameters were kept constant using a batch size of

64, a learning rate of 0.01, a sigmoid output transfer function, a cross entropy loss function, an Adam (Kingma and Ba, 2014) learning update ($\beta_1 = 0.9, \beta_2 = 0.999, \epsilon = 0.1$), and weights for encoder and decoder components were untied.

Transfer functions for hidden layers were either ReLU, ELU, or RRU functions. The subtypes of RRU were assigned symmetrically to encoder and decoder layers [R1RU, O2RU, O2RU, R1RU, O2RU, O2RU, R1RU] for fair comparisons to avoid the possibility of strategic differentiation of encoding and decoding learning components. In Figure 3, the loss (top row) and reconstruction errors (bottom row) are plotted for each the three types of networks for the training test data. The results confirm the findings of Clevert et al. (2015), who show that ELU networks show improved performance over ReLU networks for this auto-encoder architecture. However, RRU networks outperform both ELU and ReLU networks although the differences in loss cross entropies are more marginal than that of the corresponding reconstruction errors.

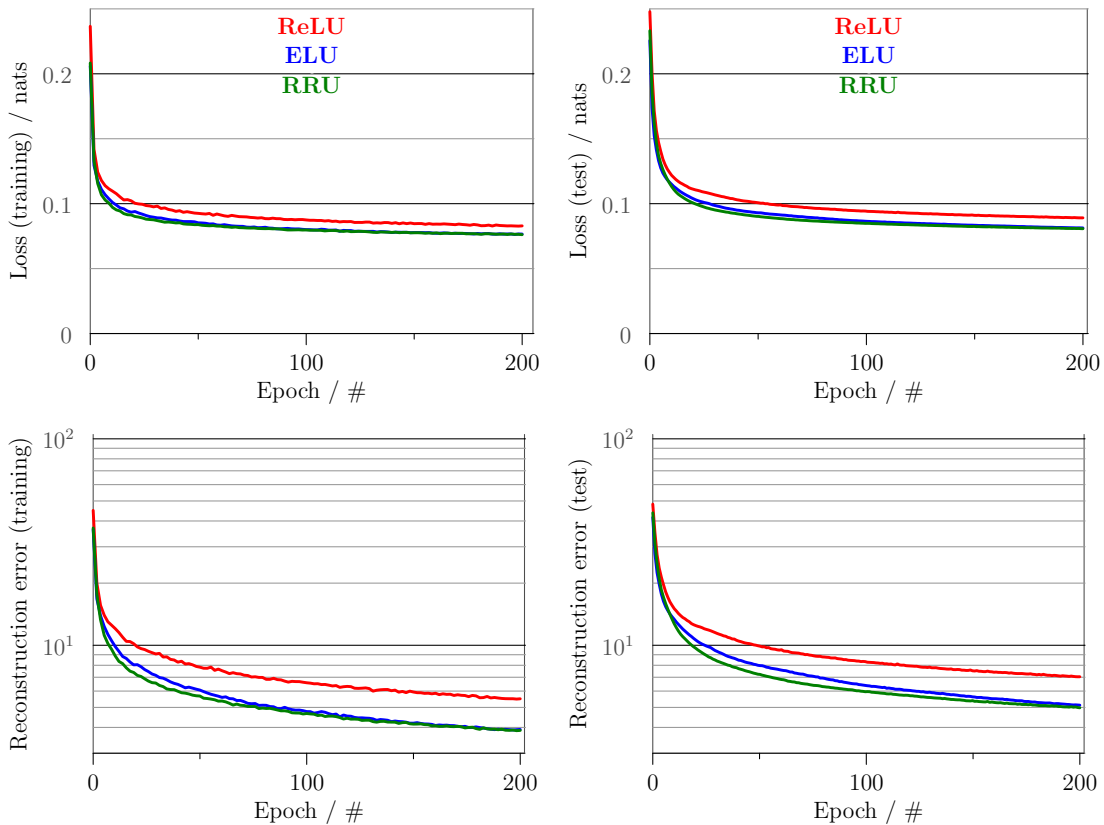


Figure 3: Stack auto-encoder training on MNIST data. Networks employing ReLU, ELU, and RRU activation functions were trained, and the loss and reconstruction errors for training and test sets from several runs are plotted as lines that represent the medians.

3.3 Convolutional network supervised learning

Since convolutional networks are specifically adapted for image processing, they constitute architectures that are well suited for the MNIST data set. A convolutional network with a simple architecture was employed to moderate computational complexity for efficient comparison in performance between the activation functions. The architecture was based on the LeNet-5 network (LeCun et al., 1998): ([6 feature maps, 5x5 convolution kernel size, 1 stride], [6 maps, 2x2 pool, 2 stride], [16 maps, 5x5

convolution, 1 stride], [16 maps, 2x2 pool, 2 stride], [120 maps, 5x5 convolution, 1 stride], 84 fully-connected).

The convolutional network was simplified from the LeNet design in three respects. First, ‘same’ padding was used throughout all convolution and pooling layers. Second, the pooling layers were conventional maximum pool layers without learnable parameters. Finally, output activations were softmax functions with losses calculated using cross entropies. Training parameters were kept constant using a batch size of 64, a learning rate of 0.01, and an Adam (Kingma and Ba, 2014) learning update ($\beta_1 = 0.9, \beta_2 = 0.999, \epsilon = 0.1$). Since maximum pooling was employed, transfer functions for convolution layers preceding pooling layers were computed only immediately after pooling layers for computational efficiency and without altering the weight initialisation procedure for RRU networks. Therefore there were only four transfer function computations within the hidden layers, which for the RRU networks were assigned as [R3RU, O2RU, O2RU, R1RU].

In Figure 4, the loss (top row) and error quotients (bottom row) are plotted for each the three types of networks for the training and test data. The results support the findings of Clevert et al. (2015), who show that ELU convolutional networks train faster than ReLU networks. However, RRU networks not only outperform both ELU and ReLU networks as measured by the training loss and error quotients, but as training progresses results in the lowest loss for the test data by some considerable margin. These results suggest that even in the absence of explicit regularisation, the intrinsic capability of RRU networks to learn generalised models exceeds that of ReLU and ELU networks.

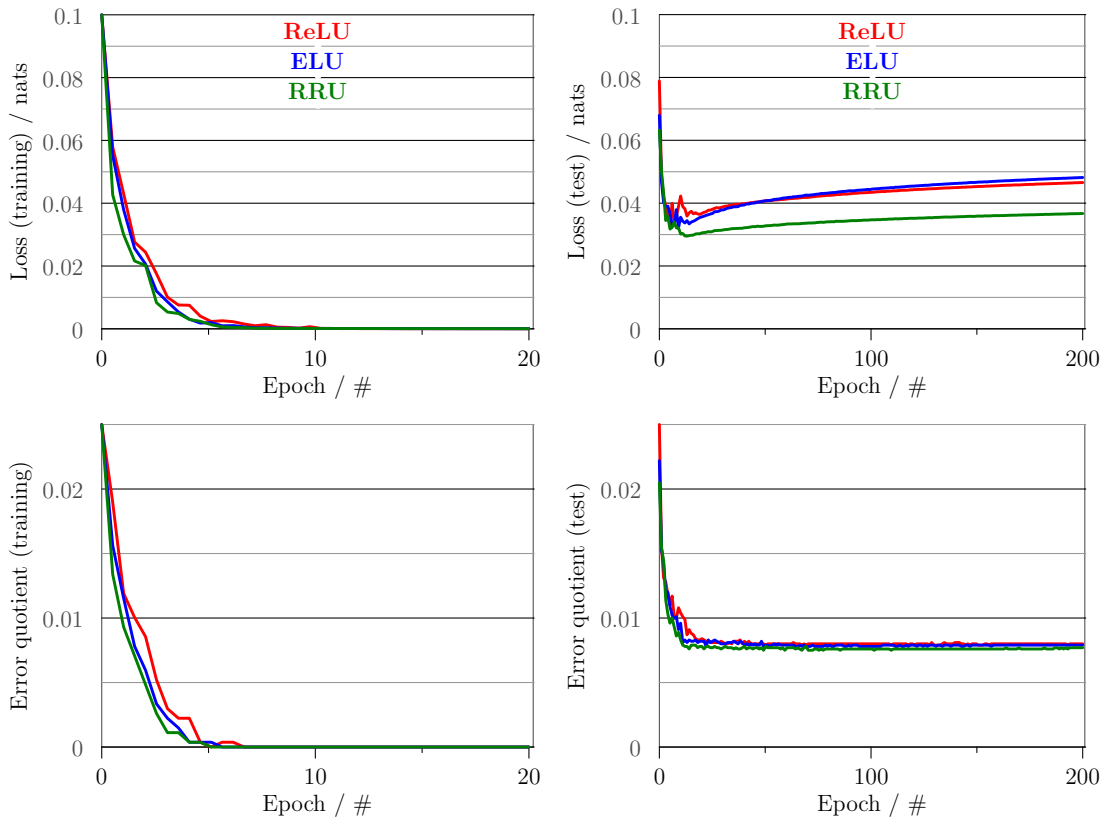


Figure 4: Simplified LeNet convolutional network training on MNIST data. Networks employing ReLU, ELU, and RRU activation functions were trained, and the loss and error quotients for the training and test sets from several runs are plotted as lines that represent the medians.

4 Discussion

The results of the present study show that RRU networks learn more quickly than their ReLU and ELU counterparts. For all hidden layers the speeds during ReLU and ELU training are limited homogeneously by the maximum of one in the activation gradient, whereas the maximum gradient for each RRU layer corresponds to its respective radix r . Differences in the non-linearities across hidden layers in effect lead to different learning speeds throughout the network. Assignment of higher radix RRU transfer functions to earlier layers therefore results in these layers naturally learning more quickly than later layers, in a manner somewhat analogous to the practice of initial pre-training of early layers.

However, not only do RRU networks learn more quickly, but also exhibit an intrinsic capacity to learn models that generalise more effectively compared to other networks. These findings might challenge the reported sparse encoding advantages attributed to the ReLU transfer function (Glorot et al., 2011). While the positive linearity in the ReLU and ELU functions may alleviate the effects of the vanishing gradient in backpropagation, it is possible that this comes at cost of the tendency to overfit as a result the gradient of one in the positive polarity remaining unchecked. In the case of the ReLU and ELU functions therefore, the solution of mitigating the vanishing gradient using a naïve linearity might be the very cause of how their resulting models are impeded in their generalisation without formal regularisation.

For the purposes of simplicity, only very few activation functions (3) from the RRRU and ORRU subfamilies were used for the present study. It is highly likely that other permutation assignments throughout hidden layers using higher radix non-linearities could improve results dramatically. Since the radix term r is continuous, a potential learning strategy would be to anneal non-linearities during the course of training to optimise learning. And while biologically-inspired empirical approaches were devised for initialising the weight coefficients, it is probable that implementation of a full theoretical framework underlying parameter initialisation for RRU layers would further ameliorate learning performance.

The suggestion that the logistic sigmoid function is ‘biological’ would reflect a somewhat incomplete understanding of the excitable properties of neuronal membranes. RRUs constitute transfer functions that are substantially more physiologically plausible than sigmoidal activations. In the experiments of the present study, RRU networks outperformed their ReLU and ELU counterparts both in terms of speed and generalisation often by considerable margins. It is perhaps true therefore in the understanding of intelligent learning that we should not only look to biology for inspiration, but for solutions.

5 Acknowledgement

The author thanks Maneesh Sahani for helpful discussion and comments on this work.

6 Appendix

6.1 Evaluation of gamma distribution shape from the radix non-linearity

Equation 3 was used to assign gamma distributed values u according the shape and scale parameters γ and λ for RRRU layers. The skew of the gamma distribution was quantified by the quotient M between the mean over the mode.

$$M = \frac{\text{mean}}{\text{mode}} = \frac{\gamma\lambda}{(\gamma-1)\lambda} = \frac{\gamma}{\gamma-1}$$

$$\therefore \gamma = \frac{M}{M-1} \quad (9)$$

The mean and mode were mapped in the parameter space for the activation function with respect to z according to the following relation:

$$\begin{aligned} \text{mean} &= z_+ - z_- \\ \text{mode} &= -z_- \end{aligned} \quad (10)$$

where $z_- = -1/e$ and z_+ is the corresponding positive value for z where the activation derivative is identical as it is for z_- . The motivation of this approach is to map the skewness, quantified by M to the relative positions of z_- and z_+ that quantify the asymmetry of the activation derivative either side of $z = 0$. The derivative at z_- can be expressed with respect to the radix r by substituting into the derivative for the negative case given in Equation 1.

$$\left. \frac{df(z)}{z} \right|_{-1/e} = r e^{-r/e} \quad (11)$$

Equating the right hand expression to the positive derivative given in Equation 1 gives the solution:

$$z_+ = \frac{\exp\left(\frac{r^2}{e(r-1)}\right) - 1}{r^2} \quad (12)$$

Finally substituting these expressions for z_+ and z_- into Equations 10 allows expression of M and therefore γ with respect to r , and the solution is given in Equation 4.

References

- Abadi M, Agarwal A, Barham P, Brevdo E, Chen Z, Citro C, Corrado GS, Davis A, Dean J, Devin M, Ghemawat S, Goodfellow I, Harp A, Irving G, Isard M, Jia Y, Jozefowicz R, Kaiser L, Kudlur M, Levenberg J, Mané D, Monga R, Moore S, Murray D, Olah C, Schuster M, Shlens J, Steiner B, Sutskever I, Talwar K, Tucker P, Vanhoucke V, Vasudevan V, Viégas F, Vinyals O, Warden P, Wattenberg M, Wicke M, Yu Y, Zheng X (2015) TensorFlow: Large-scale machine learning on heterogeneous systems Software available from tensorflow.org.
- Bhumbra GS, Bannatyne BA, Watanabe M, Todd AJ, Maxwell DJ, Beato M (2014) The recurrent case for the renshaw cell. *J Neurosci* **34**(38):12919–32.
- Bhumbra G, Beato M (2013) Reliable evaluation of the quantal determinants of synaptic efficacy using bayesian analysis. *J Neurophysiol* **109**(2):603–620.

- Binder MD, Heckman C, Powers RK (2011) The physiological control of motoneuron activity. *Comprehensive physiology* .
- Clevert DA, Unterthiner T, Hochreiter S (2015) Fast and accurate deep network learning by exponential linear units (elus). *arXiv preprint arXiv:1511.07289* .
- Dayan P, Abbott LF (2001) *Theoretical neuroscience*, Vol. 806 Cambridge, MA: MIT Press.
- Desjardins G, Simonyan K, Pascanu R et al. (2015) Natural neural networks In *Advances in Neural Information Processing Systems*, pp. 2071–2079.
- Ermentrout B (1998) Linearization of fi curves by adaptation. *Neural computation* **10**(7):1721–1729.
- Fourcaud-Trocmé N, Hansel D, Van Vreeswijk C, Brunel N (2003) How spike generation mechanisms determine the neuronal response to fluctuating inputs. *Journal of Neuroscience* **23**(37):11628–11640.
- Glorot X, Bengio Y (2010) Understanding the difficulty of training deep feedforward neural networks In *Proceedings of the Thirteenth International Conference on Artificial Intelligence and Statistics*, pp. 249–256.
- Glorot X, Bordes A, Bengio Y (2011) Deep sparse rectifier neural networks In *Proceedings of the Fourteenth International Conference on Artificial Intelligence and Statistics*, pp. 315–323.
- Hassabis D, Kumaran D, Summerfield C, Botvinick M (2017) Neuroscience-inspired artificial intelligence. *Neuron* **95**(2):245–258.
- He K, Zhang X, Ren S, Sun J (2015) Delving deep into rectifiers: Surpassing human-level performance on imagenet classification In *Proceedings of the IEEE international conference on computer vision*, pp. 1026–1034.
- Hinton GE, Salakhutdinov RR (2006) Reducing the dimensionality of data with neural networks. *science* **313**(5786):504–507.
- Hodgkin AL, Huxley AF (1952) A quantitative description of membrane current and its application to conduction and excitation in nerve. *The Journal of physiology* **117**(4):500–544.
- Kingma DP, Ba J (2014) Adam: A method for stochastic optimization. *arXiv preprint arXiv:1412.6980* .
- LeCun Y, Bottou L, Bengio Y, Haffner P (1998) Gradient-based learning applied to document recognition. *Proceedings of the IEEE* **86**(11):2278–2324.
- MacLachlan E (1975) An analysis of the release of acetylcholine from preganglionic nerve terminals. *The Journal of physiology* **245**(2):447–466.
- Murthy VN, Sejnowski TJ, Stevens CF (1997) Heterogeneous release properties of visualized individual hippocampal synapses. *Neuron* **18**(4):599–612.
- Nair V, Hinton GE (2010) Rectified linear units improve restricted boltzmann machines In *Proceedings of the 27th international conference on machine learning (ICML-10)*, pp. 807–814.
- Robinson J (1976) Estimation of parameters for a model of transmitter release at synapses. *Biometrics* pp. 61–68.
- Rosenblatt F (1958) *The perceptron: a theory of statistical separability in cognitive systems (Project Para)* Cornell Aeronautical Laboratory.
- Silver R (2003) Estimation of nonuniform quantal parameters with multiple-probability fluctuation analysis: theory, application and limitations. *J Neurosci.Methods* **130**(2):127–141.